http://dx.doi.org/10.5012/bkcs.2012.33.5.1465

Electrochemical Thinning for Anodic Aluminum Oxide and Anodic Titanium Oxide

Inhae Lee, Yunkyoung Jo, Yong-Tae Kim, Yongsug Tak,* and Jinsub Choi*

Department of Chemical Engineering, Inha University, Incheon 402-751, Korea
**E-mail: ystak@inha.ac.kr (Y. G. Tak); jinsub@inha.ac.kr (J. S. Choi)*
Received January 6, 2012, Accepted January 31, 2012

For given electrolytes, different behaviors of anodic aluminum oxide (AAO) and anodic titanium oxide (ATO) during electrochemical thinning are explained by ionic and electronic current modes. Branched structures are unavoidably created in AAO since the switch of ionic to electronic current is slow, whereas the barrier oxide in ATO is thinned without formation of the branched structures. In addition, pore opening can be possible in ATO if chemical etching is performed after the thinning process. The thinning was optimized for complete pore opening in ATO and potential-current behavior is interpreted in terms of ionic current-electronic current switching.

Key Words : Titanium oxide, Aluminum oxide, Anodization, Barrier oxide

Introduction

Anodic aluminum oxide (AAO) prepared by the anodization of aluminum in acidic media is a well-known nanotemplate material for the fabrication of nanowires and nanotubes. It's highly ordered honeycomb structures with controllable uniform diameters and lengths can be consistently produced at low cost.[1-6] Recently, researchers have found that anodization of titanium in a solution containing fluoride ions produces similar structures; the anodic titanium oxide (ATO) displays hexagonally arranged nanotubular structures with controllable length up to several hundred micrometers.[7-10]

The prepared ATO has been widely used for not only above-mentioned nanotemplates but also photoelectrochemical applications such as photoanodes and dye solar cells.[7-10]

Since many theories and methods for the fabrication of the highly ordered AAO have been studied, it would be expedient to apply knowledge of them to the fabrication of ATO. For example, pulse potential and potential shock can be successfully applied for opening the porous oxide film from the metal substrate for both AAO and ATO.[11,12]

If stepwise reduction of potential is applied to AAO, the thickness of barrier layer homogeneously decreases, producing branched structures underneath the initial barrier layer.[13-15] Step differences in potential and the final potential are key parameters to control the branch thickness. Since the thickness of barrier layer can be decreased by this method, it was called "thinning" by several groups.[15,16] The thinning process has been documented as detaching AAO from the aluminum substrate[17,18] and as a very important step in electrochemical deposition without the removal of aluminum substrate.[2,15]

This work compares the behaviors of AAO and ATO during thinning. The great differences of behavior come about as AAO is an insulator and ATO is a n-type semiconductor.[19,20] This means that ionic current is the major contributor to current flow in AAO, whereas both ionic and electronic currents can influence the formation of oxide in ATO. Based on this, morphological changes with respect to stepwise potential reduction will be interpreted with the growth and dissolution behaviors of AAO and ATO. This comparison will help to understand the differences and similarities in the formation of AAO and ATO.

Experimental Methods

All electrolytes were prepared from reagent-grade chemicals (Aldrich) and deionized water (DI water, > 18 MΩ cm). Al foils (0.25 mm, 99.99%, goodfellow) were anodized based on a two step anodization procedures using 0.3 M oxalic acid. Experimental procedures are described in detail elsewhere.[21] The first anodization was carried at 40 V in 0.3 M oxalic acid for 24 h at 13 °C - 17°C and subsequently the formed oxide was selectively removed from the aluminum substrate in chromic acid solution. Then, the second anodization was carried out at 40 V in 0.3 M oxalic acid for 1 h at 13 °C - 17 °C, making hexagonally arranged porous alumina with a thickness of 1.5 μm and a diameter of 35 nm.

TiO_2 nanotubular structures were formed from Ti foils (0.127 mm, 99.7% purity, Aldrich), which were cleaned by sonication in acetone, isopropanol (or ethanol), and DI water for 10 min each. The anodization solution was prepared from ethylene glycol (EG) containing 0.25 wt % NH_4F and 1.0 wt % DI water. Anodization of Ti was carried out using a two-step method. In the first step, titanium was anodized at 40 V at room temperature for 2 h. The formed oxide was subsequently removed using the epoxy adhesive method.[22] A second anodization was carried out at 40 V at 20 °C - 25 °C for 3 h. Titanium oxide with a thickness of 10-15 μm was fabricated through the anodization.

During anodization and thinning, the power supply (Keithley sourcemeter 2400) was used in a two-electrode

system consisting of the Al foil (or the Ti foil) as the working electrode and a Pt wire as the counter electrode. The stepwise potential from 40 V to 10 V (or 30 V or 0 V) with different rates of 0.01 V/s to 5 V/s was applied to AAO (or ATO) immediately after its fabrication.

The morphologies of the bottom were analyzed using a field emission scanning electron microscope (FE-SEM, Hitachi, S-4300). For the observation of the bottom of the barrier oxide layers in AAO, the aluminum substrate was selectively removed by a mixture of $CuCl_2$ and HCl. The epoxy adhesive method was used for bottom viewing of ATO.[22] The thickness of the walls of the titanium oxide nanotubes was measured by a field emission transmission electron microscopy (FE-TEM, JEOL, JEM 2100F). For the cross-sectional images of FE-TEM, the nanotubes were sliced to a width of approximately 70 nm by using an ultra-microtome (UTM, MTX) and the sliced samples on copper grids were dried in vacuum oven at 55 °C for 12 h before FE-TEM measurement.

Results and Discussion

Figure 1 shows bottom views of the barrier oxide of AAO after stepwise potential reduction from 40 V to 10 V with different scan rates (0.01 V/s - 5 V/s). Note that the initial AAO, which is produced at 40 V in 0.3 M oxalic acid, has hexagonal cells of around 100 nm (see the inset of Figure 1(a)).[5] Interestingly, the cells keep their size when the scan rate is 5 V/s. As scan rate decreases, the initial hexagonal patterns are destroyed, resulting in the formation of small cells (Figures 1(c) and (d)). This implies that branched structures are generated on the bottom of the pores by the slow stepwise potential reduction. Figure 2 shows the results of the thinning process in ATO conducted with identical experimental conditions as for AAO. Unlike in AAO, the barrier oxide is partially removed at high scan rates. Even though the pores are not completely opened, the total

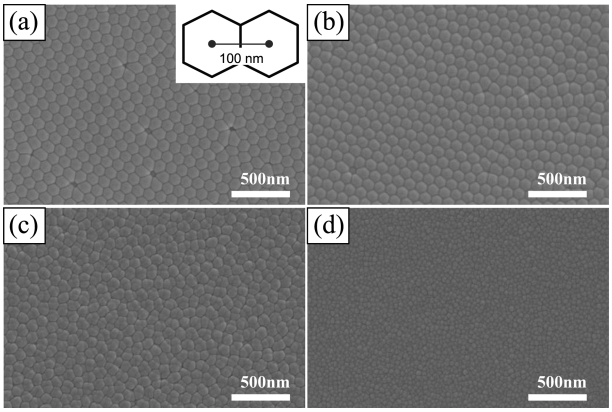

Figure 1. FE-SEM images of anodic aluminum oxide (AAO) after potential reduction from 40 V to 10 V at different reduction rates of (a) 5 V/s, (b) 1 V/s, (c) 0.1 V/s, and (d) 0.01 V/s. AAO was prepared by two-step anodization in 0.3 M oxalic acid at 5 °C and thinning was carried out in 0.3 M oxalic acid at room temperature. Note that the inset of Figure 1(a) indicates the initial cell size of AAO.

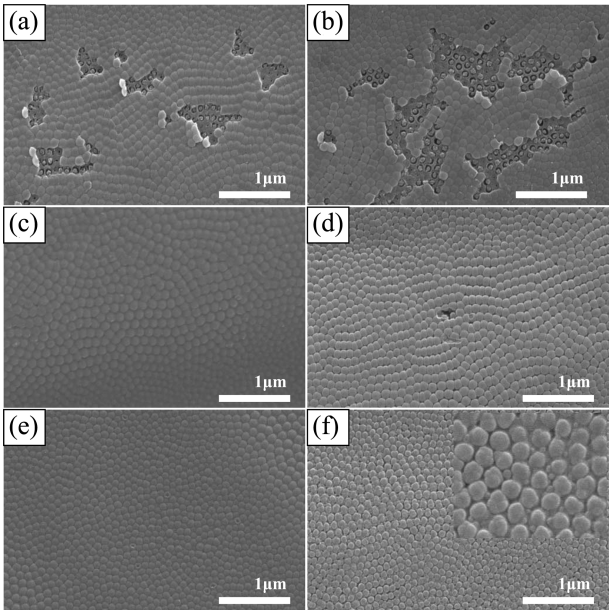

Figure 2. FE-SEM images of anodic titanium oxide after potential reduction from 40 V to 10 V at different reduction rates of (a) 5 V/s, (b) 3 V/s, (c) 2 V/s, (d) 0.5 V/s, (e) 0.1 V/s, and (f) 0.01 V/s. The formation of ATO and its thinning were carried out in ethylene glycol (EG) containing 0.25 wt % NH_4F and 1.0 wt % DI water.

number of opened pores is strongly influenced by the reduced scan rate. Inhomogeneous pore opening was only observed when the scan rate was more than 3 V/s. At moderate scan rates between 0.5 and 2 V/s, the barrier oxide exhibited a morphology similar to that of the initial structures. At extremely low scan rates nucleation of branch-like structures on the boundaries of the cells is observed (see the inset of Figure 2(f)).

Figure 3 shows current transitions in AAO and ATO as thinning proceeds. In Figure 3(a), the difference in current between before and after thinning (Δ Curr) increases as the scan rate is reduced. It indicates the size and density changes of AAO during thinning since the cell size and density are strongly influenced by the current density flowing through them. For example, the scan rates between 0.01 V/s and 0. 1 V/s destroyed arrays or produced tiny structures as seen in Figures 1(c) and (d). Similarly, for ATO, greater Δ Curr is observed at lower scan rates (Figure 3(b)). The Δ Curr in AAO was much higher than that in ATO, meaning that the size and number of AAO changed during thinning much more than that of ATO at the low scan rate. This is well correlated with the morphological observations of Figures 1 and 2.

During the formation of oxide, current is mainly ionic. Anions, such as OH^- or O^{2-}, migrate into positively charged metal and become a source of metal oxide. On the other hand, cations such as Al^{3+} or Ti^{4+} migrate into the oxide, building up the oxide layer.

$$2Al^{3+} + 3O^{2-} \rightarrow Al_2O_3 \quad (1)$$

$$Ti^{4+} + 2O^{2-} \rightarrow TiO_2 \quad (2)$$

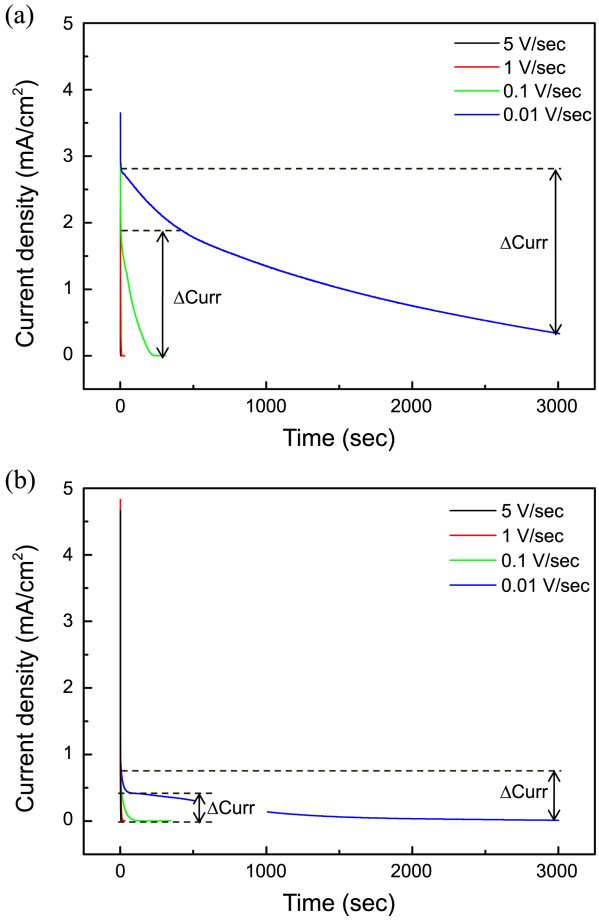

Figure 3. Current density transitions with time: stepwise reduction carried out in AAO (a) and ATO (b) at different scan rates of 5, 1, 0.1, and 0.01 V/s. ΔCurr denotes the difference between the initial and final current densities during stepwise reduction.

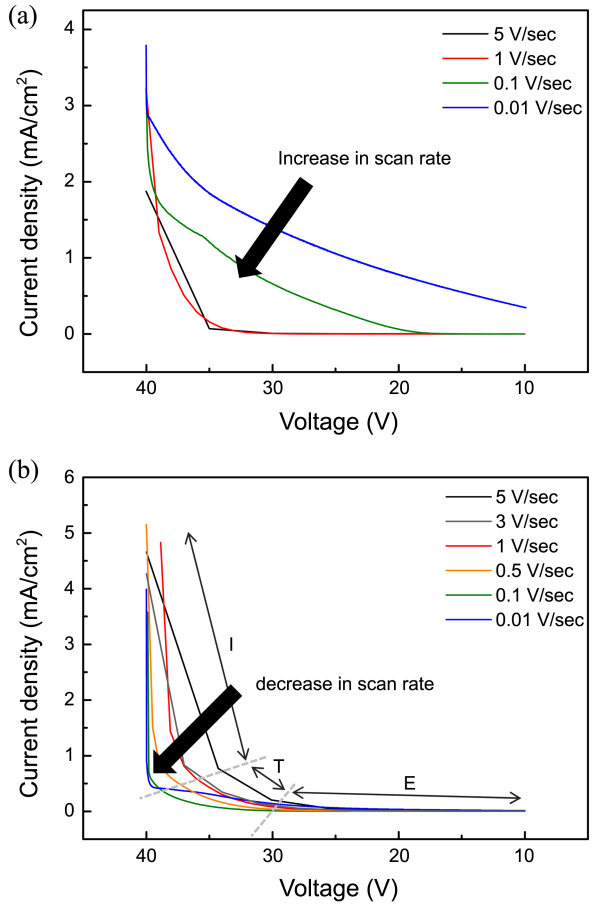

Figure 4. Current density transitions in terms of voltage: (a) AAO and (b) ATO.

The cations are ejected into the solution by chemical dissolution during the formation of oxide, making porous or tubular structures, respectively.

$$Al_2O_3 + 6H^+ \rightarrow 2Al^{3+} + 3H_2O \quad (3)$$

$$TiO_2 + 6F^- + 4H^+ \rightarrow TiF_6^{2-} + 2H_2O \quad (4)$$

It is clear that applied potential drives the current flow in the oxide, determining the ionic or electronic current components. For example, upon a sudden reduction of applied potential, the driving force is insufficient to move anions and cations through the oxide. Thus, electronic current becomes the dominant contributor to current flow. Oxide cannot be generated during the electronic current mode since the electronic current cannot carry the ions. Rather, the formed oxide is dissolved during the electronic current mode via consumption of oxygen in oxide layer, giving up electrons.[20]

$$2Al_2O_3 \rightarrow 2Al^{3+} + 3O_2\uparrow + 4e \quad (5)$$

$$TiO_2 \rightarrow Ti^{4+} + 2O_2\uparrow + 4e \quad (6)$$

As the oxide becomes thin enough again to move anions and cations by dissolution during the electronic current mode, ionic current will resume dominancy.

Figure 4 shows voltage-current density curves during stepwise potential reduction. We speculate that there are three distinguishable regions exhibited by ATO, whereas unclear regions are observed in AAO. The steep slope labeled I is where ionic current is the major contributor, and the gentle slope, T, is the transition current containing both ionic and electronic currents. The saturated slope, E, is where electronic current is the major contributor.

AAO and ATO differ because of their respective insulating semiconducting properties. Even though electronic current in AAO can flow during reduced potential by the impurity center model,[23,24] the switch from ionic to electronic current seems to be slow compared with that in ATO.[20] It means that a long transition time from ionic to electronic current inevitably exists in AAO, making the branched structures. However, the transition time can be reduced in ATO by increasing the scan rate, allowing the possibility to produce opened pores without the formation of branched structures. Only problem to produce the opened pores is that the electronic current can switch to ionic current easily in ATO since the oxygen in ATO can be consumed during the electronic current mode.[20] Therefore, before the current reverts to ionic current, the applied potential must be further reduced to maintain the electronic current. If it is well manipulated, then the pores can be opened without the formation

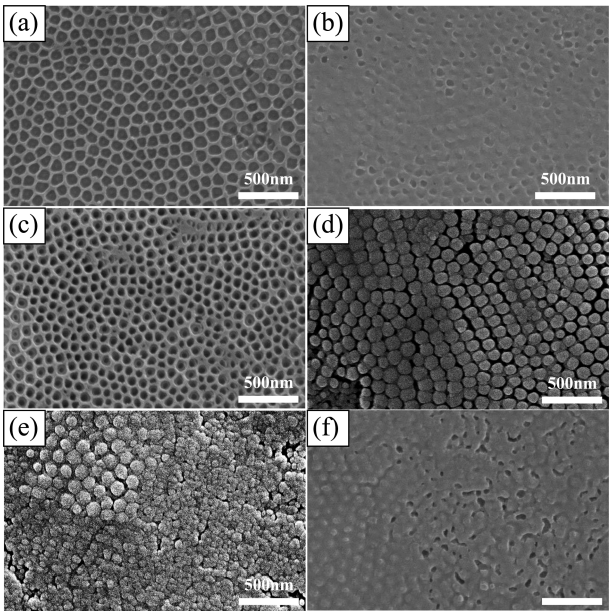

Figure 5. FE-SEM images after 1 wt % HF chemical etching of ATO. The ATO was thinned at: (a) 5 V/s, (b) 3 V/s, (c) 2 V/s, (d) 0.5 V/s, (e) 0.1 V/s, and (f) 0.01 V/s.

of the branched structures.[16]

As shown in Figure 4, current density decreases as scan rate increases in AAO, whereas the opposite is observed in ATO. This strongly indicates that AAO thinned at a low scan rate makes branched structures which enlarge the surface area for current flow. On the other hand, in the case of ATO, the high current at fast scan rates reflects that current can easily flow in the oxide. It is probably due to the titanium oxide including the barrier layer which is effectively thinned at the fast scan rate. However, as the scan rate increases,

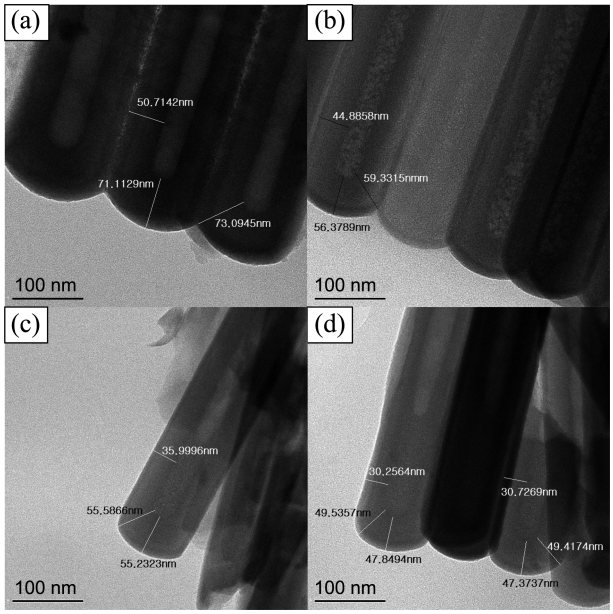

Figure 6. FE-TEM images of ATO after stepwise potential reduction at a scan rate of 2 V/s from 40 V to (b) 30 V, (c) 10 V, (d) 0 V. Note that the original ATO prepared at 40 V is shown in Figure 6(a).

Table 1. Thickness of oxide layers as a function of the finial stepwise potentials, which are determined through Figure 6

Thickness \ Final voltage	Original (40 V)	30 V	10 V	0 V
Center of barrier layer	71.2	56.4	55.2	47.5
Wall	50.7	44.9	36.0	30.5
Edge	73.1	59.3	55.6	49.4

inhomogeneous reactions at the interface increase, making the partially opened pores shown in Figure 2. In addition, the period of electronic current mode (E) would be too short at the faster scan rate (see Fig. 4). Thus, there is trade-off at an optimized scan rate for homogenous pore opening. This was found to be 2 V/sec. It was confirmed by chemical etching in HF of ATO after the stepwise reduction at 2 V/sec (Figure 5). Since TiO_2 nanotubes can be easily dissolved in HF, mild HF (here, 1 wt % HF) solution was used. The time was optimized at 1 min. As observed in Figure 5, complete opening of pores was observed in the sample thinned at the rate of 2 V/s (Figure 5(c)), meaning that the barrier oxide is homogenously thinned at this rate.

Figure 6 shows TEM images of ATO before and after stepwise potential reduction at 2 V/s, demonstrating that the barrier oxide layer can be effectively thinned by this method. Surprisingly, unlike AAO, not only the barrier oxide but also the wall of the nanotubes is thinned (See Table 1). It is generally accepted that the stepwise potential reduction in AAO does not influences the wall thickness of the pores that are determined during anodization.[15] On the other hand, the final thickness of barrier oxide layer in AAO is determined by the final potential.[2,15] Dissimilar to AAO, the barrier oxide in ATO is still thick when the thinning process proceeds down to 0 V. It can also be ascribed to the dissolution reaction at the walls, which probably consumes the dissolution current.

Conclusions

AAO and ATO were found to behave very differently when stepwise reductions of potential were applied. This is because AAO is an insulator in which ionic current mainly contributes to current flow, whereas ATO is a semiconductor in which ionic and electronic currents contribute. It was found that when stepwise potential is applied to AAO, the switch from ionic to electronic current is slow, resulting in branched structures. On the other hand, the switch is relative fast in ATO, showing the possibility of opened pores without formation of branched structures. Since the fast scan rate in the thinning of ATO shows fast switching but inhomogeneous pore opening and short periods of electronic current dominating, there is an optimized scan rate for the thinning process. It was found to be 2 V/s with subsequent chemical etching in 1 wt % HF for 1 min which forms completely opened pores in ATO without branched structures. FE-TEM images clearly showed that the homogenous dissolution of oxide in ATO occurs not only at the barrier layer but also in

the walls, which is not observed in AAO.

Acknowledgments. This work was supported by the New & Renewable Energy of the Korea Institute of Energy Technology Evaluation and Planning (KETEP) grant funded by the Korea government Ministry of Knowledge Economy (No. 20113030040010) and was supported by an Inha University Research Grant.

References

1. Suh, J. S.; Lee, J. S. *Appl. Phys. Lett.* **1999**, *75*, 2047.
2. Shingubara, S.; Nanopart, J. *Res.* **2003**, *5*, 17.
3. Wang, X.; Han, G.-R. *Microelec. Eng.* **2003**, *66*, 166.
4. Thompson, G. E.; Furneaux, R. C.; Wood, G. C.; Richardson, J. A.; Goode, J. S. *Nature* **1978**, *272*, 433.
5. Jessensky, O.; Müller, F.; Gösele, U. *Appl. Phys. Lett.* **1998**, *72*, 1173.
6. Li, A. P.; Müller, F.; Bimer, A.; Nielsch, K.; Gösele, U. *J. Appl. Phys.* **1998**, *84*, 6023.
7. Gong, D.; Grimes, C. A.; Varghese, O. K.; Hu, W.; Singh, R. S.; Chen, Z.; Dickey, E. C. *J. Mater. Res.* **2001**, *16*, 3331.
8. Ruan, C.; Paulose, M.; Varghese, O. K.; Mor, G. K.; Grimes, C. A. *J. Phys. Chem. B* **2005**, *109*, 15754.
9. Mohamed, A. E.; Rohani, S. *Energy Environ. Sci.* **2011**, *4*, 1065.
10. Paulose, M.; Shankar, K.; Yoriya, S.; Prakasam, H. E.; Varghese, O. K.; Mor, G. K.; Latempa, T. A.; Fitzgerald, A.; Grimes, C. A. *J. Phys. Chem. B* **2006**, *110*, 16179.
11. Tian, M.; Xu, S.; Wang, J.; Kumar, N.; Wertz, E.; Li, Q.; Campbell, P. M.; Chan, M. H. W.; Mallouk, T. E. *Nano Letters* **2005**, *5*, 697.
12. Jo, T.; Jung, I.; Lee, I.; Choi, J.; Tak, Y. *Electrochem. Commun.* **2010**, *12*, 616.
13. Furneaux, R. C.; Rigby, W. R.; Davidson, A. P. *Nature* **1989**, *337*, 147.
14. Zhao, X.; Seo, S.-K.; Lee, U.-J.; Lee, K.-H. *J. Electrochem. Soc.* **2007**, *154*, C553.
15. Santos, A.; Vojkuvka, L.; Pallarés, J.; Ferré-Borrull, J.; Marsal, L. F. *J. Electroanal. Chem.* **2009**, *632*, 139.
16. Kant, K.; Losic, D. *Phys. Status Solidi RRL* **2009**, *3*, 139.
17. Yuan, J. H.; Chen, W.; Hui, R. J.; Hu, Y. L.; Xia, X. H. *Electrochim. Acta* **2006**, *51*, 4589.
18. Chen, W.; Wu, J.-S.; Yuan, J.-H.; Xia, X.-H.; Lin, X.-H. *J. Electroanal. Chem.* **2007**, *600*, 257.
19. Choi, J.; Wehrspohn, R. B.; Lee, J.; Gösele, U. *Electrochim. Acta* **2004**, *49*, 2645.
20. Zhu, X.-F.; Song, Y.; Liu, L.; Wang, C.-Y.; Zheng, J.; Jia, H.-B.; Wang, X.-L. *Nanotechnology* **2009**, *20*, 475303.
21. Masuda, H.; Fukuda, K. *Science* **1995**, *268*, 1466.
22. Lim, J. H.; Hong, S.-Y.; Kang, S. J.; Doh, H.-J.; Song, J.; Choi, J. R.; Chung, K.-H.; Choi, J. *Electrochem. Commun.* **2009**, *11*, 2141.
23. Albella, J. M.; Montero, I.; Martinez-Duart, J. M. *Electrochim. Acta* **1987**, *32*, 255.
24. Vrublevsky, I.; Jagminas, A.; Schreckenbach, J.; Goedel, W. A. *Appl. Surf. Sci.* **2007**, *253*, 4680.